Original Research

A Tracking-Based Diffusion Tensor Imaging Segmentation Method for the Detection of Diffusion-Related Changes of the Cervical Spinal Cord With Aging

Wim Van Hecke, MSc,[1,2]* Alexander Leemans, PhD,[3] Jan Sijbers, PhD,[1] Evert Vandervliet, MD,[2] Johan Van Goethem, MD, PhD,[2] and Paul M. Parizel, MD, PhD[2]

Purpose: To compare region of interest (ROI)-based and diffusion tensor tractography (DTT)-based methods for evaluating diffusion properties of the spinal cord as a function of age.

Materials and Methods: Commonly, an ROI segmentation is used to delineate the spinal cord. In this work, new segmentation methods are developed based on DTT. In a first, DTT-based, segmentation approach, the diffusion properties are calculated on the tracts. In a second method, the diffusion properties are analyzed in the spinal cord voxels that contain a certain number of tracts. We studied the changes in diffusion properties of the human spinal cord in subjects of different ages. Diffusion tensor imaging (DTI) measurements of the cervical spinal cord were acquired on 42 healthy volunteers (age range = 19–87 years). The fractional anisotropy (FA), the mean diffusivity (MD), and eigenvalues (λ_1, λ_2, and λ_3) were compared for the ROI- and DTT-based segmentation methods.

Results: Our automatic techniques are shown to be highly reproducible and sensitive for detecting DTI changes. FA decreased ($r = -0.38$; $P < 0.05$), whereas MD and eigenvalues increased ($r = \pm 0.45$; $P < 0.05$) with age. These trends were not statistically significant for the ROI-based segmentation ($P > 0.05$).

Conclusion: DTT is a robust and reproducible technique to segment the voxels of interest in the spinal cord.

Key Words: spinal cord; diffusion tensor imaging; diffusion tensor tractography; aging; segmentation
J. Magn. Reson. Imaging 2008;27:978–991.

IT IS GENERALLY KNOWN that during aging nerve cells die, and that the amount of nerve tissue gradually reduces (1). Other age-related changes in the central nervous system are the swelling of the axons, the subsequent diminishing of myelin, and a decreasing quantity of the cytoskeleton (2). Although conventional MRI can detect morphological white matter (WM) changes, it can not reflect the tissue quality with respect to the WM microstructure coherence (3,4). These microstructural alterations will especially affect the local diffusion and are therefore measurable with diffusion tensor imaging (DTI). This relatively new MRI technique measures the diffusion of water molecules and provides insight into the WM structure of the central nervous system (5). Local quantitative measures can be derived from the diffusion tensor, such as the fractional anisotropy (FA), which is a normalized measure for the degree of anisotropy, and the mean diffusivity (MD), i.e., the averaged diffusion. Recent DTI studies of different pathologies are starting to use these quantitative measurements, demonstrating the potential of this in vivo and noninvasive imaging technique for detecting microstructural pathological alterations (6,7).

The spinal cord, a clinically important part of the central nervous system containing motor and sensory pathways, is an interesting anatomical WM structure, because degeneration of its microstructure has been reported in many diseases (8,9). Due to its specific nature of measuring microstructural WM alterations, DTI can be seen as an exquisite diagnostic technique for spinal cord examination. The spinal cord is surrounded by cerebrospinal fluid (CSF) where, in contrast to the brain, the gray matter (GM) is situated on the inside of the WM. Although there exists a great potential for studying spinal cord with DTI, only a limited number of works have been published regarding this topic (10–17).

It is known that several factors hamper a robust DTI study, such as physiologic and respiratory movement of the subject and the relative motion of the spinal cord itself due to the pulsation of the surrounding CSF. Furthermore, small susceptibility variations are present in the proximity of the cervical vertebrae. In addition, the relatively small diameter of the spinal cord (12 mm on average) and the restricted resolution of the diffusion tensor images (in this study, the resolution =

[1]Visionlab, Department of Physics, University of Antwerp, Antwerp, Belgium.
[2]Department of Radiology, University Hospital Antwerp, University of Antwerp, Antwerp, Belgium.
[3]Cardiff University Brain Research Imaging Center, Department of Psychology, Cardiff University, Cardiff, United Kingdom.
*Address reprint requests to: W.V.H., Vision Lab, Dept. of Physics, University of Antwerp, Universiteitsplein 1, N 1.18, B-2610 Antwerpen, Belgium. E-mail: Wim.Vanhecke@ua.ac.be
Received September 3, 2007; Accepted January 10, 2008.
DOI 10.1002/jmri.21338
Published online in Wiley InterScience (www.interscience.wiley.com).

$2 \times 2 \times 2$ mm^3) further impede a quantitative study. Indeed, it is known that a large number of voxels suffer from a partial volume effect (PVE); i.e., a combined signal originating from both the spinal cord and the CSF (18).

Previously reported DTI spinal cord studies generally employ a region of interest (ROI)-based approach to segment the spinal cord tissue (10–12,17,19,20). In 1999, the first in vivo report of the diffusion properties of the human spinal cord was published, in which only apparent diffusion coefficients and not the full diffusion tensor were calculated (19). In a subsequent DTI study of the spinal cord, diffusion information was extracted from only two diffusion-weighted images (10). In the work of Ries et al (20), a DTI study of the spinal cord was performed with a large in-plane resolution, resulting in highly anisotropic voxels. In their approach, the full diffusion tensor was calculated. Apparent diffusion coefficients were obtained from ROIs that were delineated in the middle of the sagittal spinal cord plane, in order to avoid contamination by the surrounding CSF. The first axial DTI study of the spinal cord was published by Wheeler-Kingshott et al (12), in which they segmented the whole spinal cord cross-section with ROIs to obtain FA, MD, and eigenvalues along the spinal cord. In the work of Valsasina et al (21), a DTI acquisition with highly anisotropic voxels was implemented. Only voxels originating from the central slice of the sagittal slab were incorporated in the further analysis and no ROIs were used. Mamata et al (17) investigated age-related spinal cord changes using DTI and reported both an FA decrease and an MD increase as a function of age.

To the best of our knowledge, almost all previously reported DTI studies of the spinal cord utilize an ROI-based approach to delineate the tissue of interest. Because an ROI delineation method is based on the manual selection of voxels, it is highly labor-intensive and user-dependent. Moreover, to avoid PVE-contaminated voxels in the analysis, other researchers proposed drawing very small ROIs to evaluate only the central sagittal slice of the spinal cord, thereby significantly reducing the data (21). The aim of this work is to introduce a more standardized and robust segmentation technique for the analysis and interpretation of DTI spinal cord data based on diffusion tensor tractography (DTT) (22). We demonstrate that the proposed segmentation approach outperforms the ROI-based method in terms of reproducibility and sensitivity. In order to verify the proposed methods, alterations of diffusion properties—which can occur due to morphological changes with normal aging—were studied in the human spinal cord. We believe that a profound understanding of the aging process, on the one hand, and of the quantitative spinal cord DTI results, on the other hand, are of major importance for future studies that aim to detect diffusion-related spinal cord changes in the case of different pathologies.

MATERIALS AND METHODS

Data Acquisition

Diffusion tensor measurements of the cervical spinal cord (C1–C5) were performed with a 1.5T MR scanner (Siemens, Erlangen, Germany) on 45 healthy subjects (23 male and 22 female persons), with a mean subject age of 45 with an SD of 16 years (19–87 years). An informed consent form was signed by all participants. All subjects had a normal-appearing spinal cord on conventional T2-weighted MR images and none had pathological spinal cord symptoms as reviewed by a radiologist A severe signal dropout due to ghosting or susceptibility artifacts, caused by the movement of the subject or the use of an echo-planar sequence, was observed in data sets of three subjects. These data sets were excluded from the analysis. All diffusion-weighted images were analyzed visually to check the presence of distortions in the data. Data sets were included in the analysis without the use of a specific distortion correction algorithm, when the geometric distortions were smaller than approximately one voxel.

For the analysis of the diffusion properties along the spinal cord length, the subjects were split into three groups: age <35 years (number of subjects = 12), age >35 and ≤ 50 years (number of subjects = 15), and age >50 years (number of subjects = 15).

Axial diffusion tensor images were obtained using a spin-echo–echo-planar imaging (SE-EPI) sequence with the following acquisition parameters: TR = 10.4 seconds; TE = 100 msec; diffusion gradient = 40 mT.m^{-1}; field of view (FOV) = 256×256 mm^2; matrix size = 128×128; number of slices = 30; image resolution = $2 \times 2 \times 2$ mm^3; b = 700 seconds.mm^{-2}; acquisition time = 12 minutes 18 seconds. Diffusion measurements were performed along 60 directions (+10 non-diffusion-weighted [b0] images) for a robust estimation of FA, tensor orientation, and MD (23). A combination of two elements of the circular polarization (CP) spine coil and one element of the neck coil was used. Diffusion tensor estimation, tractography, visualization, and quantitative analysis was performed with the graphical toolbox ExploreDTI (http://www.dti.ua.ac.be) (24). No specific distortion correction was applied.

Quantitative Diffusion Parameters of Interest

Several quantitative diffusion parameters were analyzed for all subjects, using different segmentation methods (which are described in the following paragraphs). The FA and MD were calculated and averaged over all selected voxels for all subjects and segmentation methods. In addition, the three eigenvalues (λ_1, λ_2, and λ_3), the ratio of the first and the second eigenvalue (λ_1/λ_2), and the ratio of the first and the third eigenvalue (λ_1/λ_3) were also computed, since it has been suggested (25) that these ratios can better differentiate between healthy and diseased subjects.

Spinal Cord Segmentation

Three segmentation techniques were investigated and their results were compared. First, the generally used ROI analysis was implemented. Second, a fiber tracking–based segmentation technique was developed, in which the results were derived from the tracts (26). Third, a hybrid segmentation (HS) approach was developed, incorporating information from both the tracts and the underlying voxels.

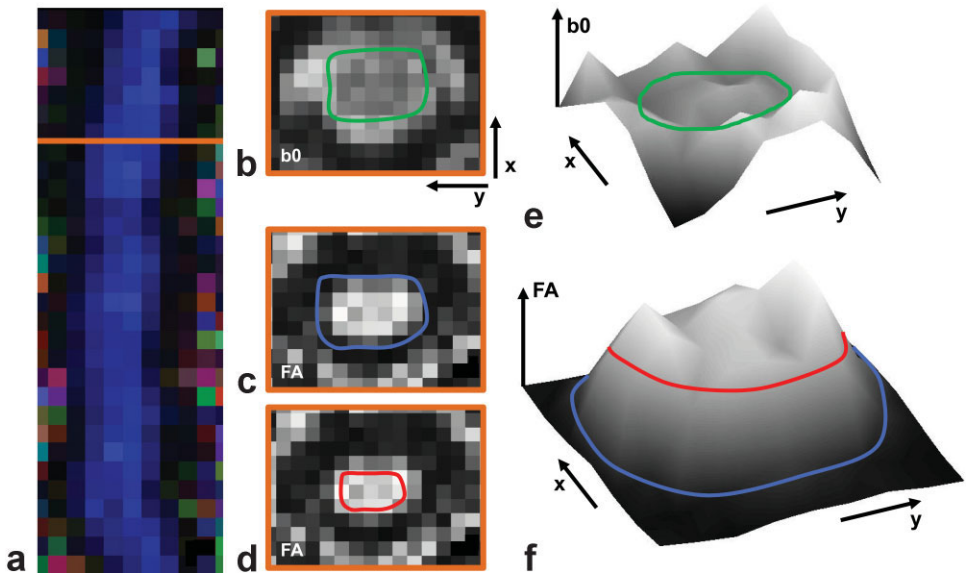

Figure 1. The spinal cord is delineated by ROIs, and the diffusion properties of the voxels inside these ROIs are evaluated. **a:** A single ROI is drawn on an axial slice and displayed on a sagittal slice. In practice, ROIs are defined on all 30 axial slices. The color in (a) encodes for the diffusion direction and the image intensity is proportional to the FA. **b:** In the b0-ROI approach, the ROI delineation was performed on the axial slices of the non-diffusion-weighted (b0) image. In the L-ROI approach, the spinal cord was covered by large ROIs, thus making sure all spinal cord data is considered. **c:** Shown by the blue ROI on the axial FA map. In the S-ROI approach, the delineation was performed with small ROIs on the FA map, containing less voxels with CSF-contaminated PVE. **d:** An example of such a small ROI is displayed in red on the axial FA map. **e**,**f:** The ROIs are also displayed on a 3D surface of the b0 values and the FA values of that same axial slice. [Color figure can be viewed in the online issue, which is available at http://www.interscience.wiley.com.]

ROI-Based Segmentation

Due to the PVE of spinal cord tissue and CSF, it is very hard to identify the edge voxels of the spinal cord. Three different ROI-based segmentation approaches, referred to as "b0-ROI," "L-ROI," and "S-ROI" are introduced that aim for an optimal selection of the spinal cord voxels. In Fig. 1a, a midsagittal slice of the spinal cord is depicted. An axial slice is selected to illustrate the three ROI-based segmentation approaches, which are visualized in Fig. 1b–d. The border voxels are included in the analysis, when their center is situated inside the polygonal.

b0-ROI

In a first approach, ROIs are manually drawn around the spinal cord on the axial slices of the b0 image (Fig. 1b). The b0 image provides a contrast that is independent of the quantitative diffusion properties that are evaluated in the subsequent analysis.

L-ROI

Since FA maps provide a better contrast between the spinal cord tissue (high FA) and the surrounding CSF (low FA), large ROIs are manually defined on axial FA slices, in this second ROI approach (Fig. 1c).

S-ROI

When large ROIs are used to select the spinal cord, PVE-contaminated voxels are included in the analysis. In an attempt to select voxels that contain only spinal cord information and no PVE with CSF, small ROIs are manually placed on the axial FA maps in this third ROI-based segmentation method (Fig. 1d).

All ROIs are drawn manually on each slice by the use of a polygonal. This was done by two observers, in order to evaluate the interobserver reproducibility.

Tracking Based Segmentation

To diminish the user-dependent factor of the ROI-based method, diffusion tensor tractography (DTT) was performed on the spinal cord that was preparatorily delineated by large ROIs, including WM, GM, and the voxels that suffer from a PVE with CSF. A standard deterministic streamline-based fiber tracking approach was applied with only one seed point per voxel in which the step size was 1 mm (27).

Subsequently, all quantitative diffusion parameters of interest are selected on the tracts (28). Note that the results of this DTT-based analysis are dependent on the interpolation technique to build the tracts, the step size, and a possible seed point interpolation factor. In the remainder of this work, we will refer to this technique as "tract based segmentation" (TS).

Compared with the ROI delineation methods, the user-dependent factor is replaced by a DTT parameter-dependency in the TS approach. It is therefore very important to choose the appropriate DTT parameters. The maximal angle between two consecutive tract points was set to 20°. Since the spinal cord is cylindrically shaped, the maximal angle between two consecutive points on the tract of 20° will not create any bias,

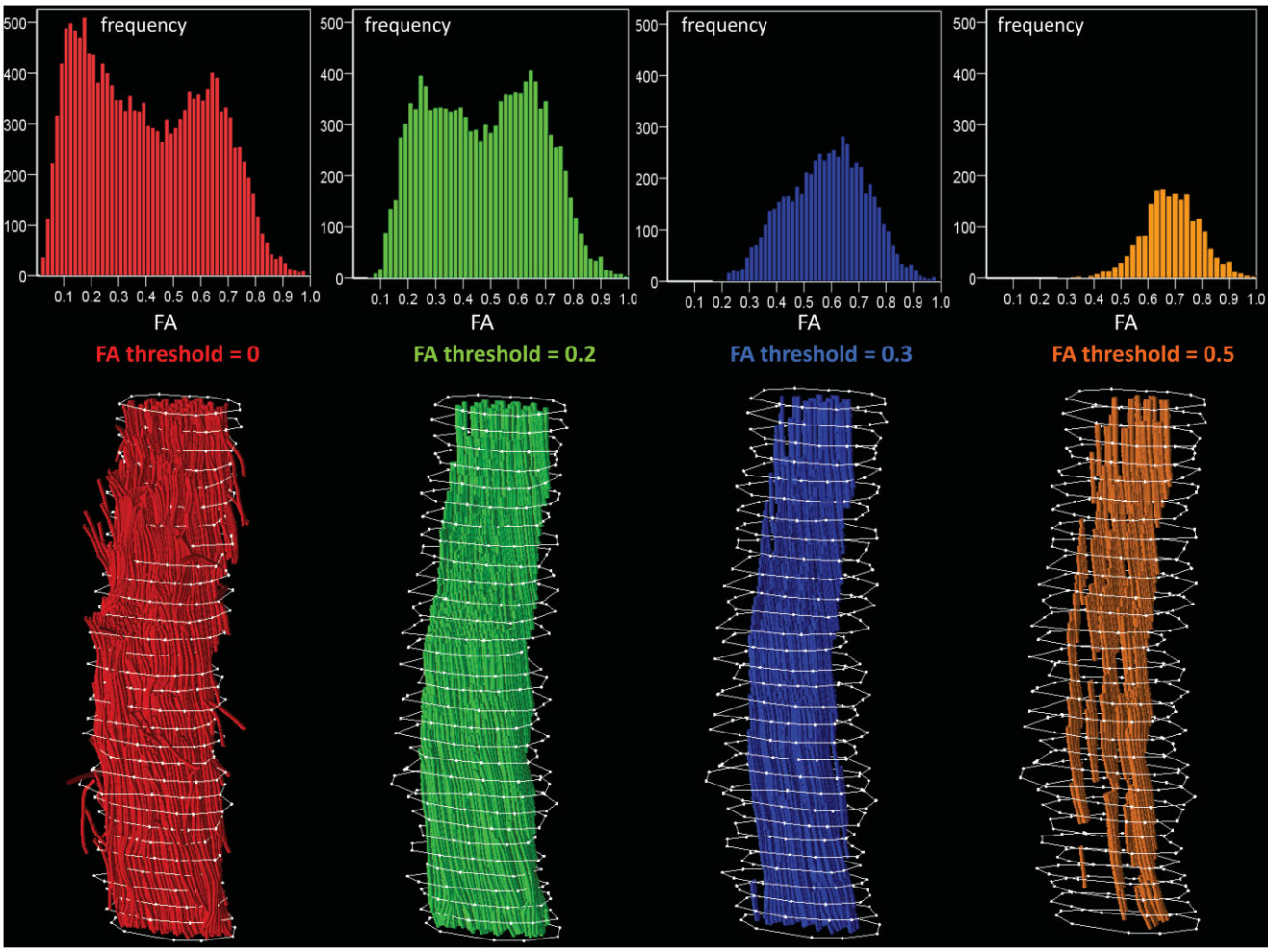

Figure 2. A qualitative tractography example and the corresponding FA histogram of the tracts are displayed for different FA thresholds on a randomly chosen subject (age 46 years). The ROIs are drawn very large around the spinal cord, including all PVE with CSF and an important part of the CSF itself. The FA threshold is the value that was used as FA for seed point selection and FA to stop tracking during the DTT algorithm. For FA thresholds lower than 0.3, an important contribution of PVE-contaminated voxels can be observed in the histograms—represented by the lower peak. Therefore, a relatively high standard error is obtained in the FA histograms. In the case of a high FA threshold (>0.6), a bias is present, since not all spinal cord voxels are included in the analysis. This can be visually detected in the tractography result. [Color figure can be viewed in the online issue, which is available at http://www.interscience.wiley.com.]

and prevents tracts from leaving the spinal cord and propagating through surrounding tissue. This was confirmed visually. On the other hand, by enforcing the tracts to have a minimal length of 5 mm, the very small tracts covering only one or two voxels are filtered out.

In the case of a low FA threshold during tracking, tracts will appear in voxels containing CSF or a PVE of spinal cord tissue with CSF. Since all tract data is included in the further analysis, this PVE-contaminated information will bias the results. Moreover, the reproducibility of the method will be worse, since less restriction is imposed by the DTT algorithm, increasing the effect of the ROI delineation on the results. On the other hand, when high FA values are chosen for the tracking procedure, only the very high anisotropic part of the spinal cord is selected. In this way, again, a bias can be introduced, because a degenerative or an older spinal cord, containing lower FA values, will not be fully taking into account and the FA will be overestimated. This bias is always present when FA thresholds are used, independent of their value, but their effect is much larger in the case of high FA thresholds. In Fig. 2, the tracts and their FA histograms of a randomly chosen 46-year-old subject are presented for different DTT FA thresholds. In our study, a value of 0.3 was observed to be optimal as a minimal FA for seed point selection and a minimal FA to stop tracking in the TS approach. When using FA thresholds lower than 0.3, the results are biased by an important presence of CSF-contaminated voxels. This FA threshold analysis was also performed on all other subjects, demonstrating analogous results, as in Fig. 2. Note that this optimal FA threshold of 0.3 can depend on the data and the study protocol.

HS Approach

This segmentation approach also employs DTT to select the spinal cord. Hereby, lower FA thresholds can be

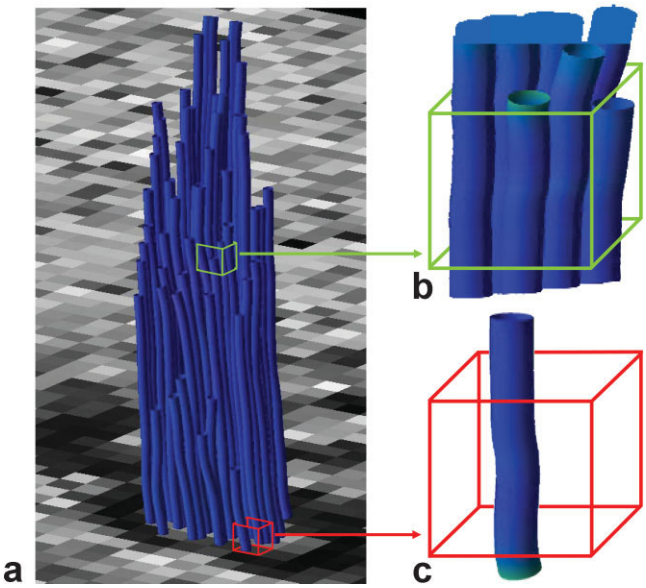

Figure 3. For each subject, DTT is performed and the tracts are visualized. Instead of evaluating the tractography results, the HS approach analyzes the diffusion characteristics in the voxels. Hereby, only voxels containing more than a specified number of tracts are included in the further analysis. **a:** A tractography result of the spinal cord and an axial FA slice. **b:** The green voxel is located at the central part of the spinal cord and contains many tracts. Therefore, the diffusion data of this voxel is included and evaluated for further analysis. **c:** The red voxel on the other hand, which is situated at the border of the spinal cord, contains only one fiber tract and the quantitative DTI parameters of this voxel are therefore excluded from the analysis. [Color figure can be viewed in the online issue, which is available at http://www.interscience.wiley.com.]

used in the DTT algorithm as compared with the TS method, since only voxels containing eight tracts—referred to as the tract threshold—are subsequently included in the analysis. In the remainder of this work, this method is referred to as "hybrid segmentation" (HS). The term "hybrid" originates from the fact that this method combines properties of the previous two methods. Indeed, DTT is performed as in the TS approach, but the diffusion parameters are evaluated on the selected voxels as in the ROI approach and not on the tracts. The HS approach is based on the idea that when many fiber tracts run through a voxel, this voxel is more reliable for the analysis. The method basically consists of two steps:

- The spinal cord is preparatorily delineated by large ROIs, including the spinal cord and the PVE with CSF. Thereafter, DTT is performed on all selected voxels, using only one seed point per voxel. Tracts with a length of 5 mm and smaller are excluded from the analysis. The maximal angle between two consecutive tracking segments is set to 20°. An FA threshold of 0.2 is used in the DTT algorithm.
- In a second step, only voxels containing a predefined number of tracts—referred to as the tract threshold—are analyzed, instead of examining all quantitative fiber tracking results, as in the TS approach (see Fig. 3).

When a high FA for seed point selection and a high FA to stop tracking are used, a bias can be introduced, as similarly stated in the TS approach. Since only voxels containing a significant amount of tracts are considered in the subsequent analysis, the effect of PVE-contaminated voxels on the results will be reduced. Therefore, a lower FA threshold could be implemented in the DTT algorithm of the HS approach, compared to TS.

The optimal tract threshold obviously depends on the FA threshold that was used in the DTT algorithm. No FA threshold or an FA threshold of 0.1 resulted in a similar number of fiber tracts in the CSF voxels, the PVE-contaminated voxels, and the spinal cord tissue voxels. In this case, applying a low tract threshold will result in the incorporation of many voxels containing CSF or a PVE with CSF. On the other hand, a high tract threshold will create a bias in the results by excluding spinal cord voxels from the analysis. An optimal FA threshold of 0.2 was found. This value was high enough to prevent too much tracking in PVE-contaminated voxels and low enough to restrict the potential bias of a high FA threshold, especially in data sets of older subjects.

A study was performed, concerning the optimal tract threshold when an FA threshold of 0.2 was used. When the tract threshold was high (>16), spinal cord voxels with a high FA were excluded and the number of selected voxels was reduced, thus increasing the standard error of the FA histogram of the selected voxels and creating a bias (Fig. 4). In the case of a small tract threshold, more voxels containing PVE with CSF are retained, again increasing the standard error of the FA histogram. An optimal tract threshold of eight was found in the analysis. This value excludes many PVE-contaminated voxels and retains as many spinal cord tissue voxels as possible. Furthermore, these thresholds resulted in the lowest standard error in the FA histogram of the selected voxels. In the case of higher FA thresholds during tracking or higher tract thresholds, this standard error rises because less voxels are selected. On the other hand, this standard error will increase with lower FA- and tract thresholds, since more PVE-contaminated voxels are included in the analysis. In Fig. 4, FA histograms and scatter plots of the number of tracts in the selected voxels (denoted as t) and the FA value of these voxels are displayed for different FA- and tract thresholds.

To summarize, the tract threshold is obtained by a qualitative analysis (a visual inspection of the tractography results), as well as a quantitative analysis (evaluation of the standard error of the FA). Again, it is important to note that the optimal parameters for a HS analysis can depend on the data and the study protocol.

Statistical Analysis Procedures

Statistical tests were performed with the SPSS analysis package (SPSS Inc., Chicago, IL, USA; http://www.spss.com). The intra- and intersubject reproducibility of the different segmentation methods was tested using the intraclass correlation coefficient (ICC). This coefficient is used to measure the interrater reliability for two or more raters and can be conceptualized as the ratio of the between groups variance to the total variance. A

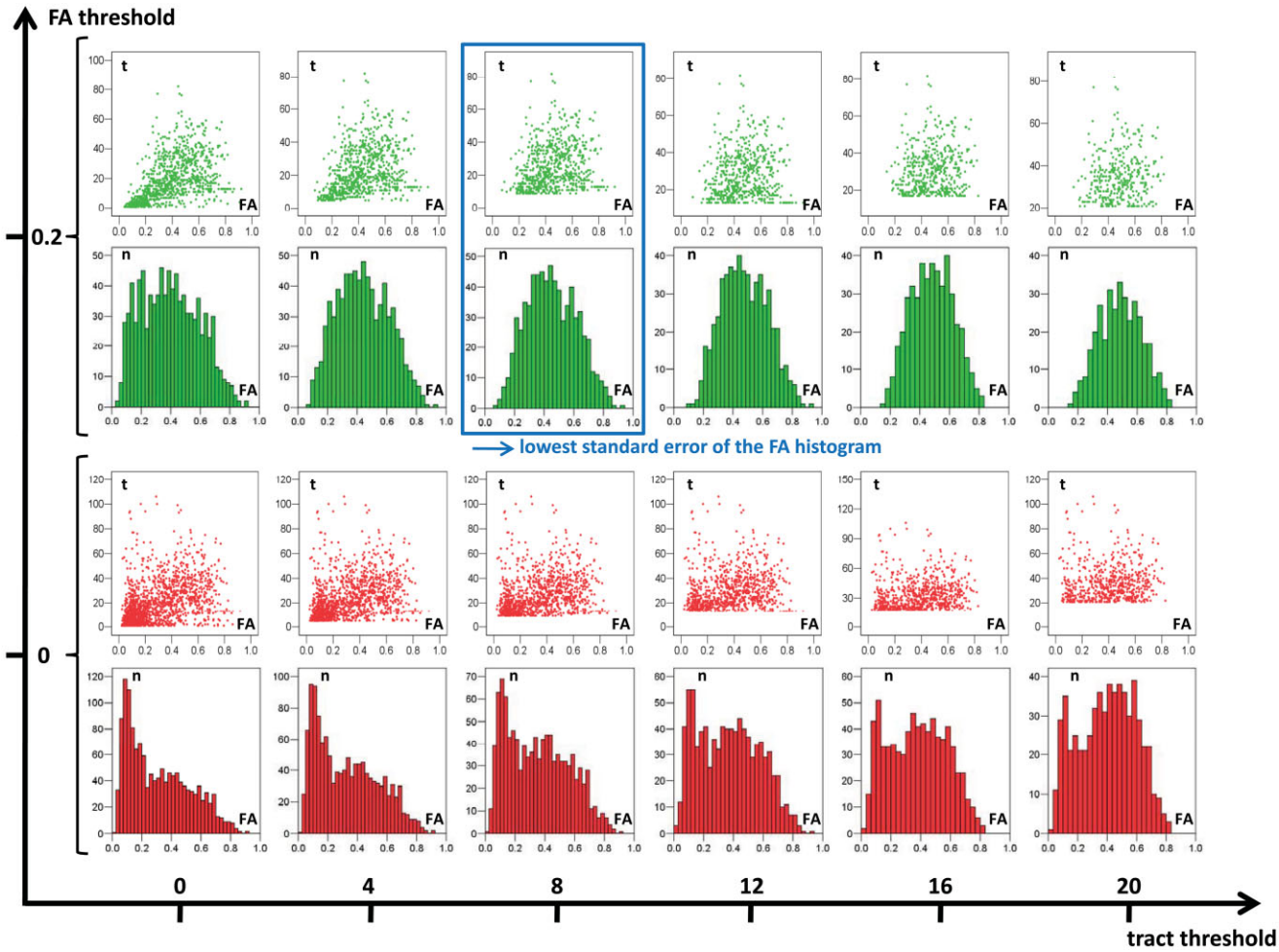

Figure 4. FA histograms and scatter plots of the number of tracts in the selected voxels (denoted as t) and the FA value of these voxels are displayed for different FA and tract thresholds on a randomly chosen person (age 48 years). The tract threshold is the minimal number of tracts that have to be present in a voxel, in order to retain that voxel in the analysis. The optimal tract threshold is dependent on the chosen FA threshold. To minimize the potential bias by considering only very high FA values in the analysis, the latter threshold is optimally as low as possible. However, it is clear that the contribution of PVE with CSF and CSF in the results is too large in the case of low FA thresholds. Consequently, to avoid these factors, the tract thresholds must be very large, thereby excluding voxels of the spinal cord. An optimal FA threshold of 0.2 was found. For this value, the tract threshold was optimally set to 8, resulting in a minimized standard error of the FA histogram. [Color figure can be viewed in the online issue, which is available at http://www.interscience.wiley.com.]

measurement is deemed highly reproducible for ICC $>$ 0.9. In the case of $0.7 <$ ICC < 0.9, the reproducibility is considered acceptable. Finally, ICC < 0.7 was interpreted as poorly reproducible.

To investigate correlations between the diffusion measurements and age, Pearson (r) and Spearman (ρ) correlation tests were performed—depending on the data distribution as investigated by the Kolmogorov-Smirnov test. Kolmogorov-Smirnov tests, checking normality, were applied in the case of the diffusion parameters for the different subjects and resulted in $P > 0.05$, suggesting a parametric approach for the correlation analysis. However, the parametric Pearson correlation test is dependent on the presence of outliers. In this study, outliers occurred and because they could be assumed as genuine values, a Spearman correlation test was also applied.

The DTI results of male and female subjects were combined, since a Mann-Whitney U-test showed no differences of all the diffusion parameters between the sexes ($P > 0.05$). Moreover, the age distribution was not significantly different for both sexes ($P > 0.05$, with 21 males vs. 19 females).

In the figures, "*" denotes statistical significance at the 0.05 level, "**" at the 0.01 level.

RESULTS

Reproducibility

The ICC values are shown in Table 1 for the different DTI parameters, demonstrating that the tracking-based methods are highly reproducible with ICC values above 0.9. ROI-based delineation of the spinal cord on the FA maps was observed to have a lower reliability. When ROIs were defined on the nondiffusion-weighted images, the reproducibility was even lower. Note that an intrarater as well as an interrater reproducibility is measured.

Table 1
ICC Coefficients for the Different Parameters λ_1, λ_2, λ_3, FA, and MD, and for the Different Segmentation Methods (Intraobserver as Well as Interobserver Reproducibility)

	b0-ROI		L-ROI		S-ROI		TS		HS	
	Intra	Inter	Intra	Inter	Intra	Inter	Intra	Inter	Intra	Inter
FA	0.36	0.28	0.67	0.62	0.69	0.66	0.96	0.91	0.97	0.96
MD	0.40	0.31	0.72	0.70	0.73	0.71	0.97	0.92	0.98	0.93
λ_1	0.54	0.40	0.75	0.72	0.70	0.68	0.97	0.93	0.98	096
λ_2	0.36	0.30	0.70	0.65	0.74	0.68	0.98	0.94	0.99	0.95
λ_3	0.30	0.28	0.70	0.65	0.70	0.66	0.98	0.92	0.99	0.96

Intra = intraobserver, Inter = interobserver.

Correlation Analysis

In this section, the correlation results, depicted in Figs. 5, 6, 7, and 8, are described. A trend line is drawn only in the case of a statistically significant correlation.

ROI-Based Segmentation

It is clear that MD, λ_1, λ_2, and especially λ_3 are higher for the L-ROI compared to the S-ROI approach. On the other hand, the FA is lower in the L-ROI approach. These results mark the presence of CSF or voxels contaminated with a PVE of CSF in the L-ROI results. Pearson and Spearman correlation tests revealed that the results derived with a large and a small ROI are positively correlated ($P < 0.001$; ρ and r values of approximately 0.5), indicating similar relative results. The DTI properties that are derived with the b0-ROI approach are positively correlated ($P < 0.001$) with both the L-ROI and the S-ROI results.

Although the diffusion tensor eigenvalues indicate some tendencies as a function of age, only λ_1 is significantly correlated in the case of b0-ROI and L-ROI, as shown in Fig. 5. In Fig. 5a, the eigenvalues from the b0-ROI delineation are displayed. Figure 5b and c show the results of the L-ROI and S-ROI segmentation methods, respectively. In Fig. 6, the correlation of FA, MD, λ_1/λ_2, and λ_1/λ_3 as a function of age is shown. No statistically significant correlations were found.

The results obtained by the S-ROI analysis contain less PVE-contaminated voxels with CSF compared with the L-ROI analysis. To further reduce the PVE in the results, Valsasina et al (21) selected only voxels coming from the central slice of the sagittal images. However, this strongly reduces the amount of data. Furthermore,

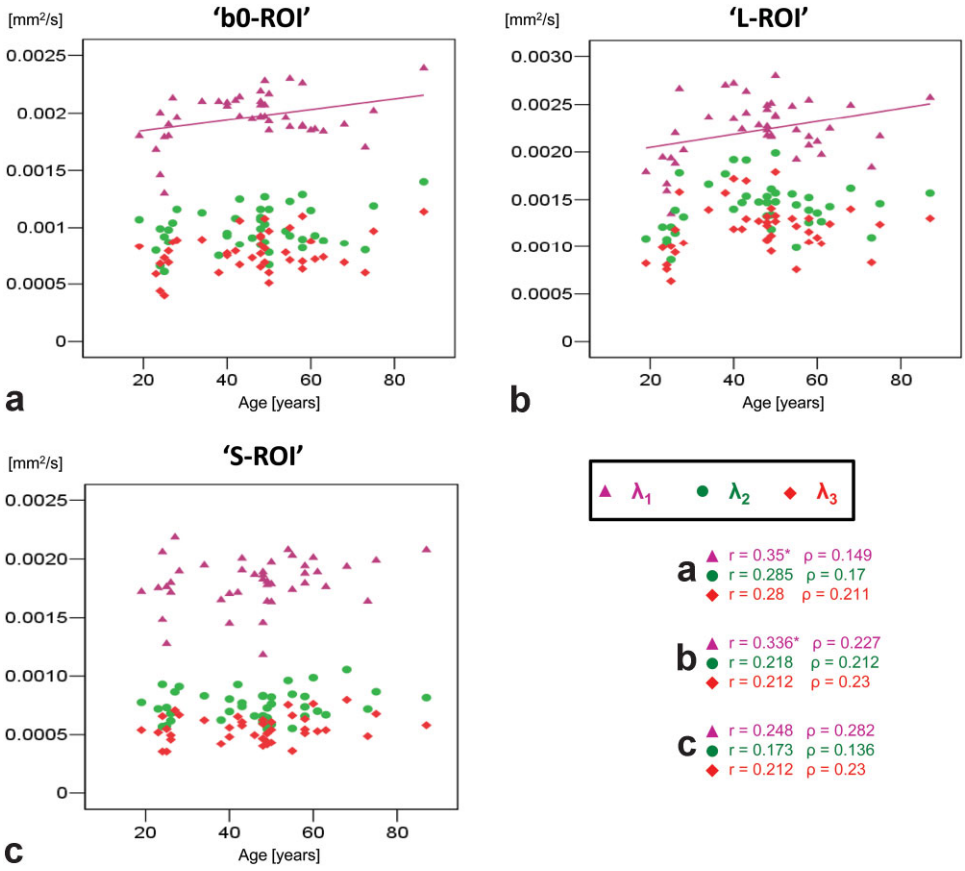

Figure 5. Correlation results of λ_1, λ_2, and λ_3 as a function of age are displayed for all ROI-based segmentation methods. **a:** The results are presented using the non-diffusion-weighted images as the contrast for the ROI delineation. Correlation results of the three eigenvalues with age, for the L-ROI- and the S-ROI-based segmentation methods on the FA maps, are visualized in (**b**), and (**c**), respectively. [Color figure can be viewed in the online issue, which is available at http://www.interscience.wiley.com.]

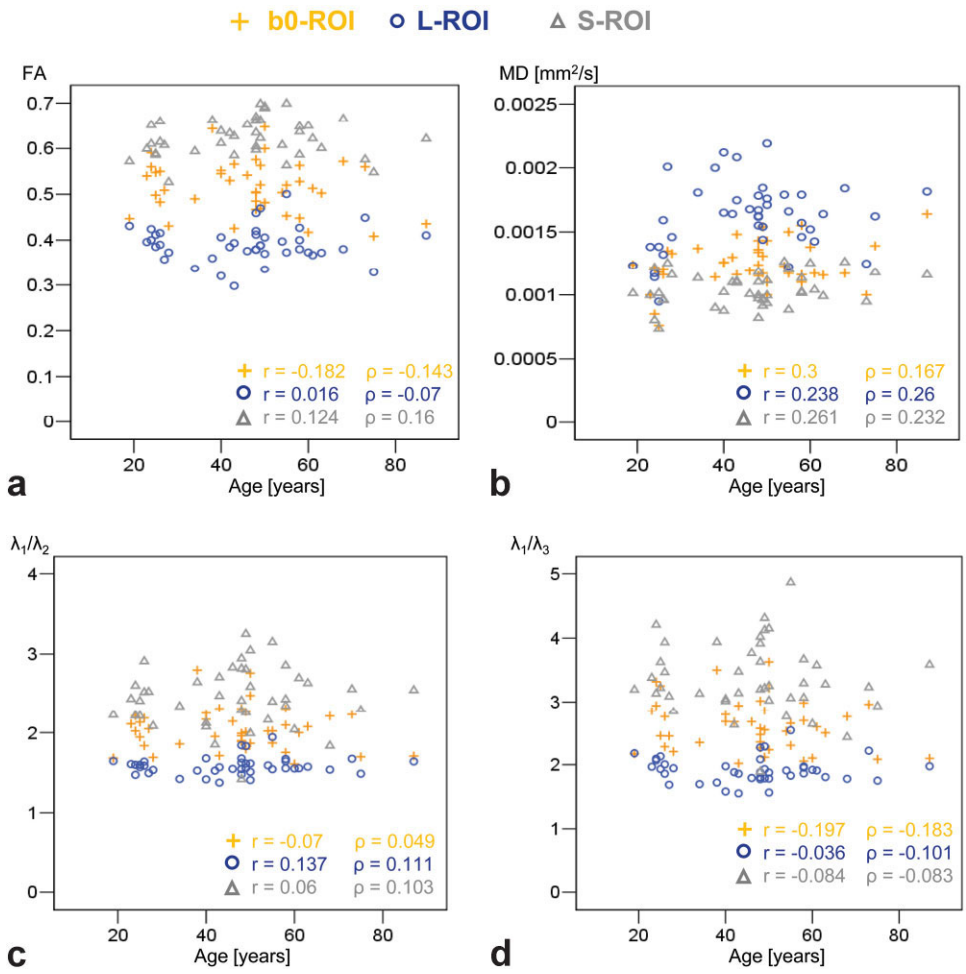

Figure 6. Correlation results of FA (**a**), MD (**b**), λ_1/λ_2 (**c**), and λ_1/λ_3 (**d**) are displayed for all ROI-based segmentation methods. The color differentiates between the three segmentation techniques. [Color figure can be viewed in the online issue, which is available at http://www.interscience.wiley.com.]

the diffusion properties of the central spinal cord voxel can differ. On the one hand, a decreased FA was observed in the central spinal cord voxels of different subjects, indicating a possible PVE of WM and GM. In some data sets, on the other hand, central voxels with a relatively high FA in the middle were noted (Fig. 7).

Tracking-Based Segmentation

The DTI parameters FA, MD, λ_1, λ_2, λ_3, and λ_1/λ_3 were found to be significantly correlated with age, when using the TS approach. λ_1/λ_2 tends to decrease with age, but not on a statistically significant basis. These results are shown in Fig. 8.

HS Approach

The correlation of all DTI parameters is statistically significant with age, and often at a $P < 0.01$ level, with $0.3 < r, \rho < 0.5$. Results are displayed in Fig. 8. The HS approach is the only segmentation method that detects statistically significant correlations for all parameters. In Fig. 8e and f it is shown that, although all three eigenvalues increase during aging, λ_2 and especially λ_3 will have a stronger effect than λ_1.

Diffusion Parameters Along the Cervical Spinal Cord Length

In Fig. 9, the diffusion properties are evaluated along the length of the spinal cord. Hereby, the HS method with the above mentioned parameters is used to select the spinal cord voxels of the different slices. The subject group was subdivided in three groups: under 35 years, between 35 and 50 years, and above 50 years. In Fig. 9a–e, the averaged diffusion parameters of the selected voxels with the HS method are calculated for each slice. Since the HS method is based on the number of tracts that run through a voxel, a small bias can be created at the edges of the image. This is due to the fact that tracts can penetrate a voxel in the middle of the image from both sides of that voxel, whereas a voxel that is situated at the edge of the image can only be penetrated along on side. A small decrease of selected voxels with the HS method was observed at the edges along three to four slices. The results of these slices are therefore deleted from the Fig. 9a–e. The trends observed in Fig. 9a–e are confirmed by an ROI analysis, as shown in Fig. 9f–j. An FA increase was found at higher cervical levels, for all age groups (Fig. 9a and f). A decrease of MD, λ_1, λ_2, and λ_3 was found for the youngest group at higher cervical levels (Fig. 9b–e). In contrast to this, these diffusion values were increasing at the higher spinal cord slices

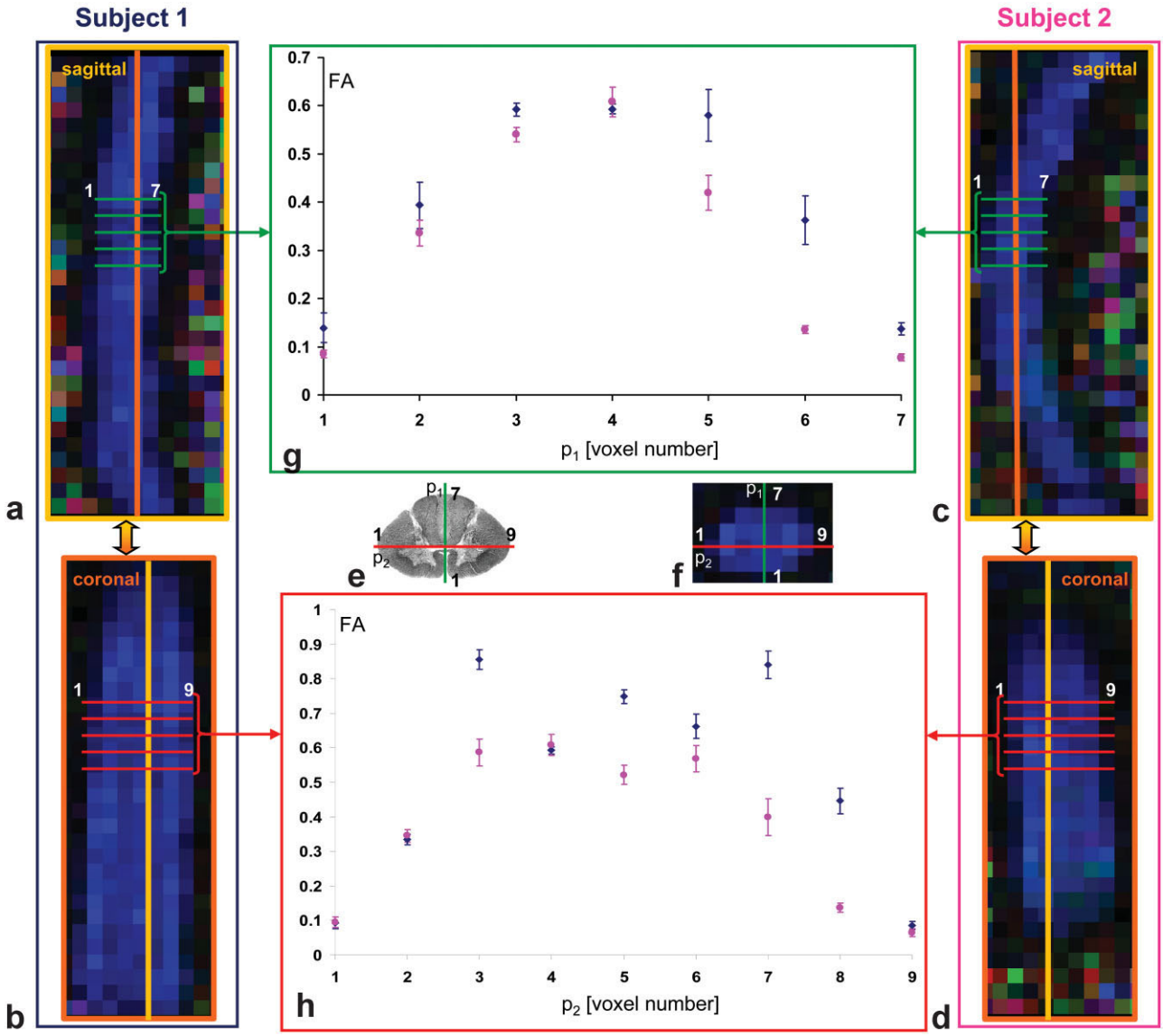

Figure 7. The cross-sectional FA dependency averaged over five axial slices is given for two subjects. In (**a**) and (**b**), the central sagittal (yellow) and coronal (orange) slice of a younger subject (35 years) are shown. In (**c**) and (**d**), the slices of the corresponding regions are displayed in the case of an older person (75 years). The color encodes for the diffusion direction and the intensity is a measure of FA. Five cross-sectional lines parallel to the axial plane were drawn, along which the FA values were analyzed. The cross-sectional lines are displayed on a histological slice (**e**) and on a diffusion tensor image (**f**) of an axial spinal cord slice. Along these lines, the numbers from 1 to 7 for the sagittal plane (p1), and from 1 to 9 for the coronal plane (p2) represent the cross-sectional voxel positions. These voxel numbers p1 and p2 can also be found in (**g**) and (**h**), where the FA values of the sagittal and coronal cross-sectional lines are presented for the younger and the older person. The error bars represent the FA variability across the five consecutive lines. The results of the younger subject (a,b) are displayed in blue, whereas the results of the older subject (c,d) are colored magenta. [Color figure can be viewed in the online issue, which is available at http://www.interscience.wiley.com.]

for the middle aged and the older group (Fig. 9b–e). These results are confirmed by the ROI analysis (Fig. 9f–j).

DISCUSSION

In this work, all subjects had a normal cervical spinal cord and no pathological spinal cord symptoms. The FA, MD, λ_1, λ_2, λ_3, λ_1/λ_2, and λ_1/λ_3 were studied as a function of age, indicating that the ROI-based segmentation method is less sensitive to age-related effects compared to the proposed tracking- or hybrid-based approaches. In the tracking-based segmentation methods (TS and HS), the user-dependent factor is negligible, but replaced by a DTT parameter dependence. Only the proposed methodology using DTT results and the underlying voxel data (HS) demonstrated a statistically significant correlation of all diffusion parameters with age. The drawback of the semiautomated approaches is that the absolute, quantitative results depend on certain parameters. The validity of the proposed methods still has to be

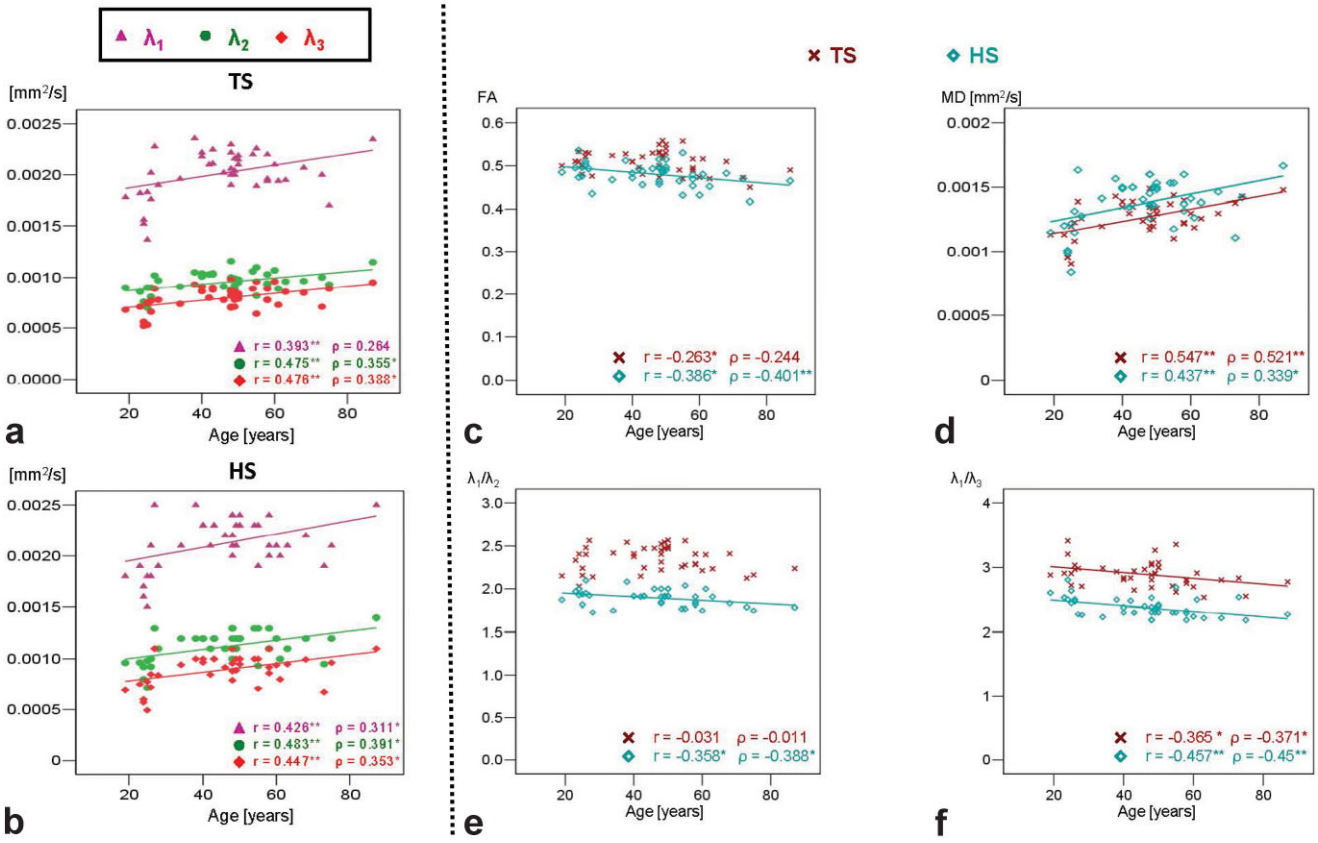

Figure 8. Correlation results of the three eigenvalues with age, for the TS and HS segmentation approaches, are visualized in (**a**) and (**b**), respectively. Trend lines are only drawn when the correlation is statistically significant. The FA (**c**), MD (**d**), λ_1/λ_2 (**e**), and λ_1/λ_3 (**f**) are displayed as a function of age for the tractography-based segmentation methods. [Color figure can be viewed in the online issue, which is available at http://www.interscience.wiley.com.]

confirmed in studies of different pathologies, which is the subject of future work.

A lot of valuable research is performed regarding the optimization of the DTI acquisition with respect to bulk motion and pulsatile flow artifacts from the surrounding CSF (16,29–32). Other studies use cardiac gating to reduce motion artifacts, or interleaved echo-planar diffusion imaging to reduce the scan time (33,34). Line scan imaging is a fast technique that relies on the acquisition of columns (30,35). However, in this work, a standard acquisition scheme was used with isotropic voxel sizes, to reduce the PVE in the slice direction. Optimized and adapted DTI acquisition schemes might improve the image quality and therefore the reliability of the subsequent analysis.

Figure 3 demonstrates that the S-ROI, L-ROI, and the b0-ROI segmentation techniques strongly suffer from a low intra- and intersubject reproducibility. The two experts that performed the segmentation were equally instructed on the ROI delineation and had no prior knowledge about the age or sex of the subjects. The lack of inter- and intrasubject reproducibility is therefore originating from a different interpretation of the data and can be seen as an indicator for the sensitive operator dependency of the ROI definition. It is clear that, when examining the spinal cord with DTI, this problem will be manifested, due to the combination of the small spinal cord size, the limited resolution, and the PVE.

TS and HS result have shown to be highly reproducible (high ICC values; see Fig. 3). The ROI definition is less stringent for TS and HS, compared to the ROI-based method, since ROIs are only used to mark out the spinal cord, including the PVE with CSF, from the surrounding vertebrae and other tissues. Furthermore, only the voxels with significant a priori information, i.e., containing a predefined number of tracts with certain anisotropy values, are evaluated in the analysis of the HS approach.

The b0-ROI, L-ROI, and S-ROI methods demonstrate correlation trends between the different DTI parameters and age (Figs. 4 and 5), but this is never considerably statistically significant. The user dependency, the small spinal cord diameter, and the PVE result in a low reliability of the ROI segmentation method, especially when ROIs are drawn on the nondiffusion weighted images. As seen in Fig. 4a and b, the b0-ROI and L-ROI approaches found a statistically significant Pearson correlation coefficient. However, this result is not confirmed by a statistically significant Spearman correlation coefficient. Therefore, the Pearson correlation significance is probably affected by the presence of outliers.

Since the ROIs are defined on the FA maps as in the L-ROI and S-ROI approaches, a potential bias can exist when studying the FA. This bias originates from the fact that FA maps are used for an ROI-based segmentation

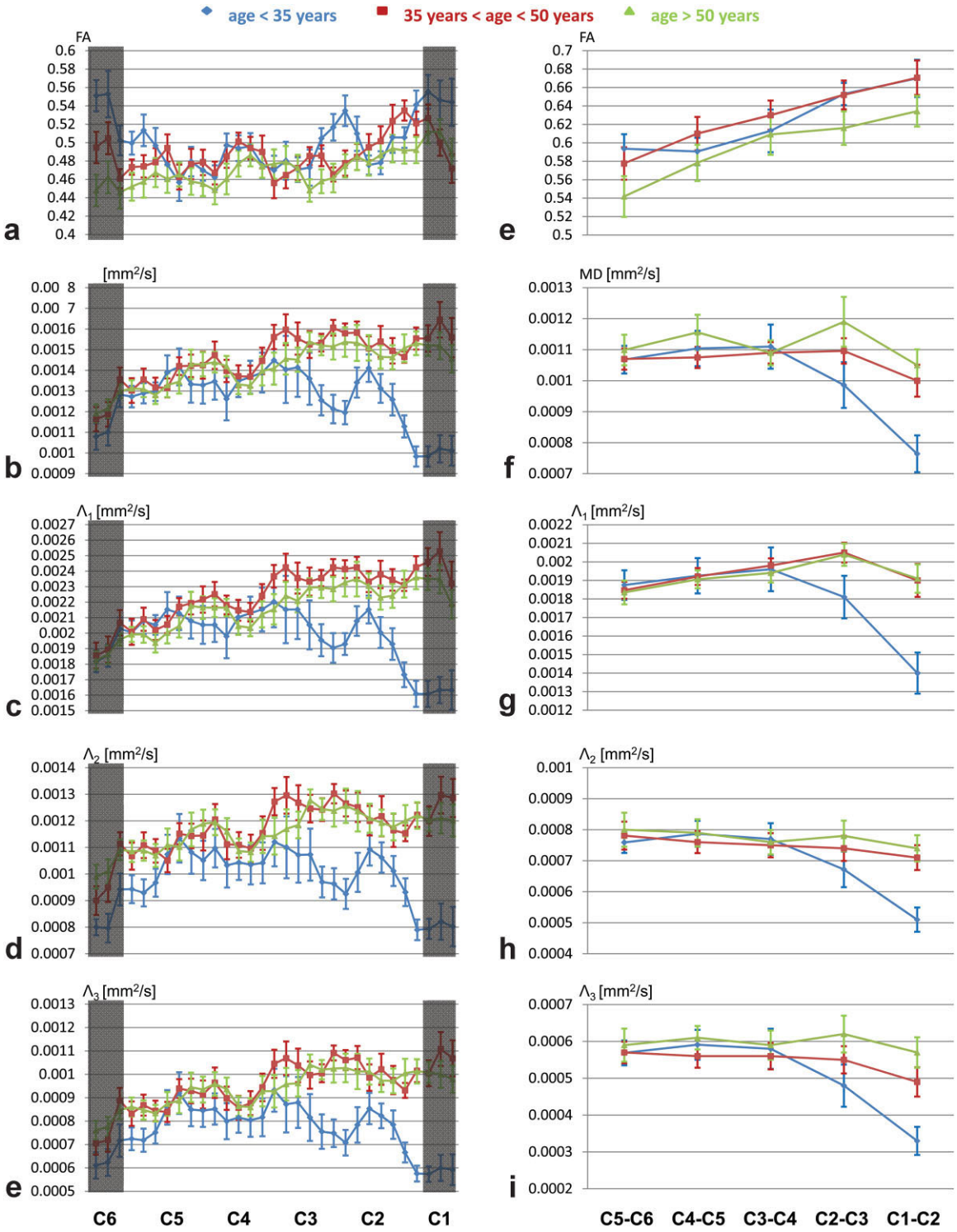

Figure 9. The diffusion properties are evaluated along the length of the cervical spinal cord (C1–C6). Hereby, the HS method is used to select the spinal cord voxels of the different slices. The subject group was subdivided in three groups: under 35 years (blue), between 35 and 50 years (red), and above 50 years (green). The FA (**a**), MD (**b**), λ_1 (**b**), λ_2 (**d**), and λ_3 (**e**) are displayed along the length of the spinal cord. [Color figure can be viewed in the online issue, which is available at http://www.interscience.wiley.com.]

of the spinal cord on the one hand, and that the FA is compared between subjects on the other hand. Spinal cord voxels with a lower FA value, for example in the case of a pathology, can therefore potentially be excluded from the analysis since they are interpreted as non-spinal-cord voxels or PVE-contaminated voxels during the ROI delineation on the spinal cord FA map. More succinctly, the dependent variable is used to define the independent variable in the analysis, which is statistically not correct. However, when an unrelated

image contrast such as the non-diffusion-weighted image (b0) is used for the ROI delineation, results are biased by a lack of reproducibility (see Fig. 3). We therefore believe the FA map presents a more adequate image contrast for an accurate ROI definition, when diffusion tensor (DT) images are acquired with the acquisition parameters of this study. Furthermore, the possible bias caused by the ROI delineation on the FA maps will not affect the quantitative results in the L-ROI method, since all spinal cord tissue and the PVE with CSF is included in the analysis. The results obtained by the S-ROI analysis contain less PVE-contaminated voxels with CSF compared with the L-ROI analysis. Valsasina et al (21) selected only voxels coming from the central slice of the sagittal images in order to reduce this PVE with CSF. As shown in Fig. 7, the DT properties of the central spinal cord voxel can vary. A possible explanation is the variation in spinal cord diameter between different subjects. Indeed, a smaller spinal cord diameter might result in a more important PVE of WM and GM, thus reducing the anisotropy values in certain voxels. Since it is reported that the spinal cord narrows and the spinal cord diameter decreases with age, only interpreting these central voxels, might affect the age-related results (36). In addition to the aging effects on the spinal cord diameter, cervical cord atrophy is a frequent finding in different pathologies (37).

The tractography results were observed to be more reproducible, since the manual ROI segmentation is only required to differentiate the spinal cord tissue and CSF roughly from the surrounding vertebrae and other tissues (see Fig. 3). Although results can be biased by the DTT parameter selection, when using tractography to select the spinal cord voxels, no such bias was observed in our study. A visual inspection confirmed that tracts were observed along the spinal cord ROI (C1–C5). Diffusion measures were compared in the case of three different DTT parameter sets for all subjects. A correlation analysis and an ICC measurement was performed comparing the results of the TS segmentation approach under different DTT parameters. Pearson and Spearman correlation coefficients were larger than 0.85 and an ICC $>$ 0.9 was found, demonstrating the high reliability of the TS approach and the rather high insensitivity of the diffusion results to the DTT parameter selection. In the case of all DTT parameter sets, a statistically significant correlation with age was observed for the diffusion parameters λ_1, λ_2, λ_3, and MD.

However, when subject groups suffering from certain degenerative spinal cord pathologies are studied, the DTT parameter selection has to be approached very cautiously. Nevertheless, we believe that, because of the much higher standardization of the tractography based method—each data set is treated in exactly the same way—its results are more reliable compared to the results of the manual ROI-based segmentation.

In the HS approach, only voxels containing a eight tracts—referred to as the tract threshold—were analyzed. The results of the HS segmentation method are, similar to those of the TS approach, parameter-dependent instead of user-dependent. Analogous to the TS segmentation, the quantitative diffusion results were compared in the case of three different FA and tract thresholds for all subjects. Again, a correlation analysis and an ICC measurement was performed, comparing the results of the HS method under different threshold values. Pearson and Spearman correlation coefficients were larger than 0.82 ($P < 0.001$) and an ICC $>$ 0.9 was found. These results indicate a high reliability of the HS approach and the rather insensitivity of the diffusion results to the threshold selection. In the case of all DTT parameter sets, a statistically significant correlation with age was observed for all the diffusion parameters λ_1, λ_2, λ_3, MD, FA, λ_1/λ_2, and λ_1/λ_3.

We postulate that the HS approach is a segmentation method that retrieves the available spinal cord information in the most reproducible and robust way.

A drawback of all implemented approaches to selecting the spinal cord voxels of interest is the fact that the diffusion properties are averaged along the cervical spinal cord (C1–C6). Wheeler-Kingshott et al (12) demonstrated that these diffusion values (FA, MD, eigenvalues) could vary along the spinal cord. They used a ROI analysis on four subjects. In Fig. 7, the FA, MD, and the eigenvalues are evaluated along the spinal cord (C1–C6). The HS method was used to select the spinal cord voxels of the different slices. The healthy subject group was subdivided in three groups according to the age. In contrast to the results of Wheeler-Kingshott et al (12), high FA values were observed at C1. Many factors can attribute to these contradictory results. First of all, Wheeler-Kingshot et al (12) used anisotropic voxels and a different acquisition scheme compared to our study. Also, the analysis of Wheeler-Kingshot et al (12) was based on four subjects, which can affect the results. Furthermore, in their study the most superior slices were at the level of the pons, where different conditions arise, i.e., less monodirectionally-oriented fibers in comparison to the spinal cord.

The HS method is based on the number of tracts that run through a voxel. Therefore, a small bias can be created at the edges of the image, due to the fact that tracts can penetrate a voxel in the middle of the image from both sides of that voxel, in contrast to voxels at the edges of the image. Therefore, the results of the three outermost slices at both edges are withdrawn from this analysis.

In contrast to the work of Wheeler-Kingshott et al (12), we subdivided our healthy population into three age groups. As Fig. 7b–e demonstrates, the MD, λ_1, λ_2, and λ_3 decreased at higher cervical levels in the youngest age group, whereas these values increased in the other two age groups. These results are confirmed by an ROI analysis along the spinal cord (Fig. 7f–j). A higher penetration of CSF through the spinal cord in older subjects can explain these findings, although other factors, such as a broadening of the spinal cord diameter at the upper levels in the younger subject group compared to the older groups, might also explain the decrease of the MD and the eigenvalues at the upper spinal cord levels in the youngest group. However, no statistically significant correlation was observed between the number of selected voxels in the different segmentation approaches and the age ($P > 0.6$ for all segmentation approaches).

The DTI results of the different segmentation methods should be interpreted with care, since no histological and thus no ground-truth data of the examined persons is available. This stresses the importance of animal studies, in which the measurement of diffusion properties can be correlated with histological findings (38). It is therefore impossible to consider one of the segmentation techniques as a perfect match with the real, underlying situation. Consequently, the objective in this study was not to determine the absolute, quantitative spinal cord DTI parameters, but to find the most reliable and robust segmentation method that can extract the relevant information, given the mentioned problematic nature of spinal cord DTI.

When the tendencies of the different DTI parameters are compared for the different segmentation methods, a certain similarity can be observed (Figs. 4, 5, and 6). This suggests that, independent of the segmentation approach used, the diffusion parameters indeed evolve as a function of age. The fact that these underlying trends of the diffusion characteristics are only detected on a statistically significant basis by the proposed HS approach, reflect the high reproducibility, sensitivity, and robustness of this segmentation method. In addition, our DTI results are confirmed by the histological findings in literature of spinal cord degeneration with aging (39). Furthermore, these tendencies are validated by the available DTI literature of both brain and spinal cord (17,40–43). Ota et al (40) detected a statistically significant increase of MD, λ_2, and λ_3 values and a decrease of the FA in function of age in most parts of the corpus callosum. They did not observe a significant increase of λ_1. Another age-related DTI study of the brain demonstrated a decreased FA, and an increased MD as a function of age in frontal fiber systems, whereas only small differences were detected in the posterior regions of the brain (41). Salat et al (42) presented analogous results. Yoshiura et al (43) discovered an FA increase in younger adults, whereas no age-related changes were observed in indices derived from MD maps. In their study, Mamata et al (17) detected an FA decrease ($r = -0.244$) and an apparent diffusion coefficient increase ($r = 0.242$) as a function of age in cervical spondylosis patients with a normal spinal cord at the C2–C3 level. The data were derived after an ROI-based delineation, whereby only the strictly central part of the spinal cord was delineated in an attempt to exclude any CSF.

In conclusion, different spinal cord DTI segmentation methods were compared in this study. We can conclude that the tendencies that were observed match with the expected evolution of the diffusion characteristics during normal aging. We demonstrate an increase of λ_1, λ_2, λ_2, MD, and a decrease of FA, λ_1/λ_2, and λ_1/λ_3 as a function of age. HS is the only segmentation method that traces the tendencies of all considered diffusion properties on a statistically significant basis. We postulate that the HS approach retrieves the available spinal cord information in the most reproducible and robust way, given the specific problematic nature of the spinal cord DTI data.

REFERENCES

1. Morrison JH, Hof PR. Life and death of neurons in the aging brain. Science 1997;278:412–419.
2. Peters A. The effects of normal aging on myelin and nerve fibers: a review. J Neurocytol 2002;581–593.
3. Albert M. Neuropsychological and neurophysiological changes in healthy adult humans across the age range. Neurobiol Aging 1993; 14:623–625.
4. Guttman CRG, Jolesz FAD, Kikinis R, et al. White matter changes with normal aging. Neurology 1998;50:972–978.
5. Basser PJ, Jones DK. Diffusion-tensor MRI: theory, experimental design and data analysis—a technical review. NMR Biomed 2002; 15:456–467.
6. Taylor WD, Hsu E, Ranga K, et al. Diffusion tensor imaging: background, potential, and utility in psychiatric research. Biol Psychiatry 2004;55:201–207.
7. Schocke MFH, Seppi K, Esterhammer R, et al. Trace of diffusion tensor differentiates the Parkinson variant of multiple system atrophy and Parkinson's disease. Neuroimage 2004;21:1443–1451.
8. Rocca MA, Hickman SJ, Bo L, et al. Imaging spinal cord damage in multiple sclerosis. J Neuroimaging 2005;15:297–304.
9. Valencia MP, Castillo M. MRI findings in posttraumatic spinal cord Wallerian degeneration. Clin Imaging 2006;30:431–433.
10. Clark CA, Werring DJ, Miller DH. Diffusion imaging of the spinal cord in vivo: estimation of the principal diffusivities and application to multiple sclerosis. Magn Reson Med 2000;43:133–138.
11. Clark CA, Werring DJ. Diffusion tensor imaging in spinal cord: methods and applications—a review. NMR Biomed 2002;15:578–586.
12. Wheeler-Kingshott CA, Hickman SJ, Parker GJ, et al. Investigating cervical spinal cord structure using axial diffusion tensor imaging. Neuroimage 2002;16:93–102.
13. Barker GJ. Diffusion-weighted imaging of the spinal cord and optic nerve. J Neurol Sci 2001;186:1:S45–S49.
14. Toosy AT, Werring DJ, Orrell RW, et al. Diffusion tensor imaging detects corticospinal tract involvement at multiple levels in amyotrophic lateral sclerosis. J Neurol Neurosurg Psychiatry 2003;74: 1250–1257.
15. Agosta F, Benedetti B, Rocca MA, et al. Quantification of cervical cord pathology in primary progressive MS using diffusion tensor MRI. Neurology 2005;64:631–635.
16. Maier SE, Mamata H. Diffusion tensor imaging of the spinal cord. Ann NY Acad Sci 2005;1064:50–60.
17. Mamata H, Jolesz FA, Maier SE. Apparent diffusion coefficient and fractional anisotropy in spinal cord: age and cervical spondylosis-related changes. J Magn Reson Imaging 2005;22:38–43.
18. Pfefferbaum A, Sullivan EV. Increased brain white matter diffusivity in normal adult aging: relationship to anisotropy and partial voluming. Magn Reson Med 2003;49:953–961.
19. Clark CA, Barker GJ, Tofts PS. Magnetic resonance diffusion imaging of the human cervical spinal cord in vivo. Magn Reson Med 1999;41:1269–1273.
20. Ries M, Jones RA, Dousset V, et al. Diffusion tensor MRI of the spinal cord. Magn Reson Med 2000;44:884–892.
21. Valsasina P, Rocca MA, Agosta F, et al. Mean diffusivity and fractional anisotropy histogram analysis of the cervical cord in MS patients. Neuroimage 2005;26:822–828.
22. Mori S, van Zijl PCM. Fiber tracking: principles and strategies—a technical review. NMR Biomed 2002;15:468–480.
23. Jones DK. The effect of gradient sampling schemes on measures derived from diffusion tensor MRI: a Monte Carlo study. Mag Reson Med 2004;51:807–815.
24. Leemans A, Sijbers J, Parizel PM. A graphical toolbox for exploratory diffusion tensor imaging and fiber tractography. 14th Annual Meeting of the Section for Magnetic Resonance Technologists (SMRT), Miami, FL, USA, 2005.
25. Song SK, Yoshino, Le TQ, et al. Demyelination increases radial diffusivity in corpus callosum of mouse brain. Neuroimage 2005; 21:132–140.
26. Jones DK, Travis AR, Eden G, et al. PASTA: pointwise assessment of streamline tractography attributes. Magn Reson Med 2005;53: 1462–1467.

27. Basser PJ, Pajevic S, Pierpaoli C, et al. In vivo fiber tractography using DT-MRI data. Magn Reson Med 2000;44:625–632.
28. Jones DK, Catani M, Pierpaoli C, et al. Age effects on diffusion tensor magnetic resonance imaging tractography measures of frontal cortex connections in schizophrenia. Hum Brain Mapp 2006; 27:230–238.
29. Bammer R, Fazekas F, Augustin M, et al. Diffusion-weighted MR imaging of the spinal cord. AJNR Am J Neuroradiol 2000;21:587–591.
30. Robertson RL, Maier SE, Mulkern RV, et al. MR line-scan diffusion imaging of the spinal cord in children. AJNR Am J Neuroradiol 2007;21:1344–1348.
31. Chou M-C, Lin Y-R, Huang T-Y, Wang C-Y, et al. FLAIR diffusion-tensor MR tractography comparison of fiber tracking with conventional imaging. AJNR Am J Neuroradiol 2005;26:591–597.
32. Carballido-Gamio J, Xu D, Newitt D, et al. Single-shot fast spin-echo diffusion tensor imaging of the lumbar spine at 1.5 and 3 T. Magn Reson Imaging 2007;25:665–670.
33. Summers P, Staempfli P, Jaermann T, et al. A preliminary study of the effects of trigger timing on diffusion tensor imaging of the human spinal cord. AJNR Am J Neuroradiol 2006;27:1952–1961.
34. Zhang J, Huan Y, Qian Y, et al. Multishot diffusion-weighted imaging features in spinal cord infarction. J Spinal Disord Tech 2005; 18:277–282.
35. Maier SE. Examination of spinal cord tissue architecture with magnetic resonance diffusion tensor imaging. Neurotherapeutics 2007; 4:453–459.
36. Ishikawa M, Matsumoto M, Fujimura Y, et al. Changes of cervical spinal cord and cervical spinal canal with age in asymptomatic subjects. Spinal Cord 2003;41:159–163.
37. Stevenson VL, Leary SM, Losseff NA, et al. Spinal cord atrophy and disability in MS: a longitudinal study. Neurology 1998;51:234–238.
38. De Boy CA, Zhang J, Dike S, et al. High resolution diffusion tensor imaging of axonal damage in focal inflammatory and demyelinating lesions in rat spinal cord. Brain 2007;130:2199–2210.
39. Morrison LR. The effect of advancing age upon the human spinal cord. Cambridge, MA: Harvard University Press; 1959.
40. Ota M, Obata T, Akine Y, et al. Age-related degeneration of corpus callosum measured with diffusion tensor imaging. Neuroimage 2006;31:1445–1452.
41. Pfefferbaum A, Adalsteinsson E, Sullivan EV. Frontal circuitry degradation marks healthy adult aging: evidence from diffusion tensor imaging. Neuroimage 2005;26:891–899.
42. Salat D, Tuch D, Greve D, et al. Age-related alterations in white matter microstructure measured by diffusion tensor imaging. Neurobiol Aging 2005;26:1215–1227.
43. Yoshiura T, Mihara F, Tanaka A, et al. Age-related structural changes in the young adult brain shown by magnetic resonance diffusion tensor imaging. Acad Radiol 2005;12:268–275.